

NEW AUTOMATED CLOUD AND CLOUD-SHADOW DETECTION USING LANDSAT IMAGERY

Kustiyo^{1*}, Dianovita¹, Hedi Ismaya¹, Mulia Ina Rahayu¹, and Erna Sri Adiningsih¹

¹Remote Sensing Technology and Data Center,
National Institute of Aeronautics and Space (LAPAN)

*e-mail: kuslapan@yahoo.com

Abstract. Cloud cover has become a major problem in the use of optical satellite imageries, particularly in Indonesian region located along equator or tropical region with high cloud cover almost all year round. In this study, a new method for cloud and cloud shadow detection using Landsat imagery for specific Indonesian region was developed to provide a more efficient and effective way to detect clouds and cloud shadows. Landsat Top of Atmosphere (TOA) reflectance and Brightness Temperature (BT) were used as inputs into the model. The first step was to detect cloud based on cloud physical properties using albedo and thermal bands, the second step was to detect cloud shadows using the Near Infrared (NIR), and Short Wave Infrared (SWIR) bands, and finally, the geometric relationships were used to match the cloud and cloud shadow layer, before proceeding to the production of the final cloud and cloud shadow mask. The results were then compared with other method such as tree base cloud separation. It showed that method we proposed could provide better result than tree base method, the accuracy result of this method was 98.75%.

Keywords: *Landsat, Cloud pixel, Potential cloud pixel, Cloud shadow*

1 INTRODUCTION

Many Landsat images especially in Indonesia as tropical area were inevitably covered by cloud (Asner, 2001). The presence of clouds and their shadows complicated the use of data in the optical domain from earth observation satellites. The brightening effect of the clouds and the darkening effect of cloud shadows affected data analyses such as inaccurate atmospheric correction, biased estimation of Normalized Difference Vegetation Index (NDVI) values, error in land cover classification, and false detection of landcover change. Therefore, clouds and cloud shadows were significant sources of noise in the Landsat data, and their detection was an initial step for further analyses (Arvidson *et al.*, 2001; Irish, 2000; Simpson and Stitt, 1998). Generally, clouds could be divided into two categories: thick opaque clouds and thin semi transparent clouds. The thick opaque clouds were relatively easier to identify because of their high reflectance in the visible bands. While, the identification of thin semi-transparent clouds became more difficult since the signals involved both from clouds and the surface underneath (Gao and Kaufman, 1995; Gao *et al.*, 1998, 2002).

Due to the high spectral variability of clouds, cloud shadows, and the earth's surface, automated accurate separation of clouds and cloud shadows from normally illuminated surface conditions is difficult. Intuitively, it seems that clouds and cloud shadows are easily separated from clear-sky measurements because clouds are generally white, bright, and cold while cloud shadows are usually dark. Nevertheless, there are clouds that are not white, bright, or cold and cloud shadows even brighter than the average surface reflectance. The problems arose from the wide range of reflectances and temperatures observed on the surface (Irish, 2000). One common approach was to screen clouds and cloud shadows manually. However, this approach was time consuming and would limit efforts to the Landsat historical study of the earth's surface.

Over the years, a number of methods were developed for cloud identification. However, most of them were designed for moderate spatial resolution sensors such as Advanced Very High Resolution Radiometer (AVHRR) and Moderate Resolution Imaging Spectro-radiometer (MODIS). These sensors were usually equipped with more than one thermal band, or with water vapor/CO₂

absorption bands, both of which were useful for thin semi transparent cloud detection (Ackerman *et al.*, 1998; Derrien *et al.*, 1993; Saunders and Kriebel, 1998). For high spatial resolution sensors like Landsat, with only one thermal band and 6 optical bands placed in atmospheric windows, an accurate cloud identification was difficult and cloud shadow identification was even more difficult. Clouds cast shadows on any type of land cover. When cloud shadows fall on urban or bright rocks, they can be very bright compared to the average surface reflectance. Moreover, when the cloud is semi transparent, the darkening effect of the cloud shadow can be subtle, making the cloud shadow hard to detect. Therefore, clouds and cloud shadows detection especially thin clouds and their shadows in Landsat images is still an important issue in the remote sensing community, particularly as we try to use increasingly automated methods to analyze large volumes of data.

Historically, screening of clouds in Landsat data was performed by the Automated Cloud Cover Assessment (ACCA) system (Irish, 2000; Irish *et al.*, 2006). By applying a number of spectral filters, and depending heavily on the thermal infrared band, ACCA generally worked well for estimating the overall percentage of clouds in each Landsat scene, which was its original purpose. However, it did not provide sufficiently precise locations and boundaries of clouds and their shadows to be useful for automated analyses of time series of Landsat images. Additionally, ACCA failed to identify warm cirrus clouds (Irish, 2000; Irish *et al.*, 2006). Wang *et al.* (1999) proposed the use of two multi-temporal Landsat TM images to identify clouds and their shadows by image differencing. This method could successfully provide an accurate cloud and cloud shadow mask, but it was highly dependent on the input images. The Landsat Ecosystem Disturbance Adaptive Processing System (LEDAPS) atmosphere correction tool also generated an internal cloud mask using two passes (Vermote and Saleous, 2007). There were

four tests in the first pass and a thermal test in the second pass which was similar to ACCA, except that the second pass generated a cloud mask while the second pass of ACCA only provided the percentage of cloud cover. This algorithm needed other ancillary data like the surface temperature provided from National Centers for Environmental Prediction (NCEP) to help generate a coarse resolution surface temperature reference layer for cloud detection. This algorithm has already been used extensively for atmospheric correction of Landsat images and has shown a better method for cloud detection in low and middle latitudes compared to ACCA. However, it might not work well when the clouds cover a large percentage of the image (large amount of leakage were observed) or in sun glint and turbid water conditions (Vermote, 2010). Hégarat-Masclé and André (2009) developed an approach that uses only two bands, Green and Short Wave Infrared (SWIR), to generate a “clear-sky line” and use the distance from the tested points to this line to detect cloud pixels. This method was originally used by Zhang *et al.* (2002) to correct for haze in Landsat imagery. It was shown to be accurate for retrieving clouds over vegetated areas, but it failed when the surface reflectance was bright, as in the case for rocks, sand, etc. (Zhang *et al.*, 2002). By implementing a cloud-mask algorithm originally developed for the MODIS Land bands on Landsat data, Oreopoulos *et al.* (2011) proposed an algorithm that performs on par with the ACCA algorithm without using the thermal band.

Detecting cloud shadow was more difficult than detecting cloud. Previously, cloud shadow identification was based on spectral tests. Though it worked sometimes, most of the time it would inevitably include other dark surfaces that had similar spectral signatures (like topographic shadows or wetlands) and excluded cloud shadows that were not dark enough (Ackerman *et al.*, 1998; Hutchison *et al.*, 2009). Recently, geometry-based cloud shadow detection was shown to be feasible and more accurate.

Currently, there are three kinds of geometry-based cloud shadow detection methods in the literature i.e., object matching, lapse rate, and scattering differencing. The object matching algorithm detects cloud shadow by matching cloud shadows with cloud objects (Berendes *et al.*, 1992; Hégarat-Masclé & André, 2009; Simpson and Stitt, 1998; Simpson *et al.*, 2000). The lapse rate method used a constant lapse rate to estimate cloud top height by brightness temperature and use the cloud pixels to cast shadows (Vermote and Saleous, 2007). This later method worked well for thick clouds but it was not accurate enough for semi transparent clouds in which the brightness temperature was a mixture of thin cloud and the surface. As cloud shadow scattering was stronger in the short wavelengths (especially Blue band), Luo *et al.* (2008) proposed to use the physical characteristics of scattering differences between the short wavelength and NIR or SWIR combined with the geometry, to produce cloud shadow masks. This new method worked well over vegetated area, but it was less accurate when the cloud shadow falls on bright surfaces or the cloud shadow comes from a very thin cloud.

In this paper, we propose a new algorithm to detect both clouds and cloud shadows for Landsat TM and Enhanced Thematic Mapper Plus (ETM+). The cloud mask was computed from albedo and thermal band from Landsat imagery to separate cloud pixel, potential cloud pixels, and clear-sky pixels. Soil index and water index were used to evaluate potential cloud pixels to clear-sky pixels or cloud pixel to produce cloud layer. Cloud shadows mask were computed from the Near Infrared (NIR) band to generate a potential shadow layer. By comparing cloud layer and shadow layer using spatial relation, shadow must be within cloud and cloud must be within shadow. The spatial relation between cloud pixel location and cloud shadow pixel location

was determined by the view angle of the satellite sensor and the type of cloud.

The need for effective and efficient cloud and shadow screening has grown tremendously for two major reasons. First, the Landsat L1T format provides accurate registration of images that they can be compiled into a time series with no significant problem in registration issues. Second, Landsat data policy change enables a free access to the archive. With such an easy way to obtain free Landsat data, the big volumes of data archives need a more efficient and effective method of data processing, particularly cloud masking, before the data could be used further. Although there is a bulk of satellite data archives, it is still difficult to obtain cloud free imageries of many areas in Indonesia. Therefore, the objective of this study was to develop a cloud and cloud shadow masking method to be applied on Landsat imageries using a combined algorithm of visible and thermal bands. The advantage of this method was that we can set the thresholding value for specific Indonesia region. A comparison with tree-base algorithm method was also conducted. By combining several approaches of existing methods, this method was developed based on specific geographic and climate condition in Indonesia, in which cloud cover has become major problem to obtain cloud free satellite data. The ultimate goal was to provide an automated method for screening clouds and their shadows for a big data volumes of Landsat imageries.

2 MATERIALS AND METHOD

2.1 Cloud and cloud shadow detection algorithms

The input data for the model were Top of Atmosphere (TOA) reflectances for Bands 1, 2, 3, 4, 5, 7 and Band 6 Brightness Temperature (BT) (Table 1). For Landsat L1T imageries, Digital Number (DN) values were converted to TOA reflectances and BT (in Celsius degree) with the sun correction software developed by CSIRO for Indonesia's National Carbon Accounting

Table 1. Landsat TM/ETM and spectral band characteristics.

Landsat TM		Landsat ETM	
Band Number	Wavelength (μm)	Band Number	Wavelength (μm)
Band 1	0.45–0.52	Band 1	0.45–0.515
Band 2	0.52–0.60	Band 2	0.525–0.605
Band 3	0.63–0.69	Band 3	0.63–0.69
Band 4	0.76–0.90	Band 4	0.75–0.90
Band 5	1.55–1.75	Band 5	1.55–1.75
Band 6	10.40–12.50	Band 6	10.40–12.50
Band 7	2.08–2.35	Band 7	2.09–2.35

System (INCAS). Then, based on cloud and cloud shadow physical properties were used to extract a potential cloud layer and a potential cloud shadow layer. Finally, the geometric relationships were used to match the potential cloud and cloud shadow layer, before proceeding to the production of the final cloud and cloud shadow mask.

There were three components of cloud pixel analysis based on spectral characteristics of the pixels i.e., thermal, albedo, and infrared bands. Different thresholds were applied to distinguish cloud and shadow pixels from bare and water pixels. Several steps using albedo or visible spectrum were used since there are several types of clouds such as thin clouds (cirri forms), thick clouds (cumuli forms), strati form, and vertical clouds (cumulonimbus). Water pixels were sometimes difficult to separate from shadow pixels. Therefore, the technique be-came complex and the critical aspect was to define the thresholds. The complete procedures to generate the cloud and shadow masking is described in Figure 1.

2.2 Layers of potential clouds and cloud shadows

2.2.1 Potential cloud layer

The first step in the algorithm combined several spectral tests to identify the potential cloud pixels (the pixels that may be cloudy or may be clear). Otherwise, the pixels were considered to be absolutely clear-sky pixels, or absolutely cloud pixels.

The first pass included a number of spectral tests as follows:

- if $f(X)_{thick} \leq X_{thick-low}$, then P = absolutely clear-sky pixels;
- if $X_{thick-low} < f(X)_{thick} < X_{thick-up}$, then P = potential cloud pixels;
- if $X_{thick-up} \leq f(X)_{thick}$, then P = absolutely cloud pixels;
- if $f(X)_{temp} < X_{temp-thres}$, then P = absolutely cloud pixels;
- if $X_{temp-thres} < f(X)_{temp}$, then P = absolutely clear-sky pixels;

where:

cloud thickness function:

$$f(X)_{thick} = (X_1 + X_2 + X_3)/3,$$

X_i : Digital number fixel of band -i of Landsat data

cloud temperature function:

$$f(X)_{temp} = X_6;$$

X_6 : Temperature derived from band 6 of Landsat data

$X_{thick-low}$ =lower threshold value of cloud thickness

$X_{thick-up}$ =upper threshold value of cloud thickness

$X_{temp-thres}$ =threshold value of cloud temperature

P = pixel

This “Basic Test” was one of the fundamental tests for cloud identification. Due to the bright and cold nature of clouds, bright cloud was detected by mean of visible band, and cold clouds was detected by temperature from band 6 of Landsat data. After that, the potential cloud pixels must be classified into absolute clear-sky pixels or absolutely cloud pixels. Two tests for potential cloud pixels were applied. First was soil test, and second was confidence test close to cloud with distance. Soil test was to

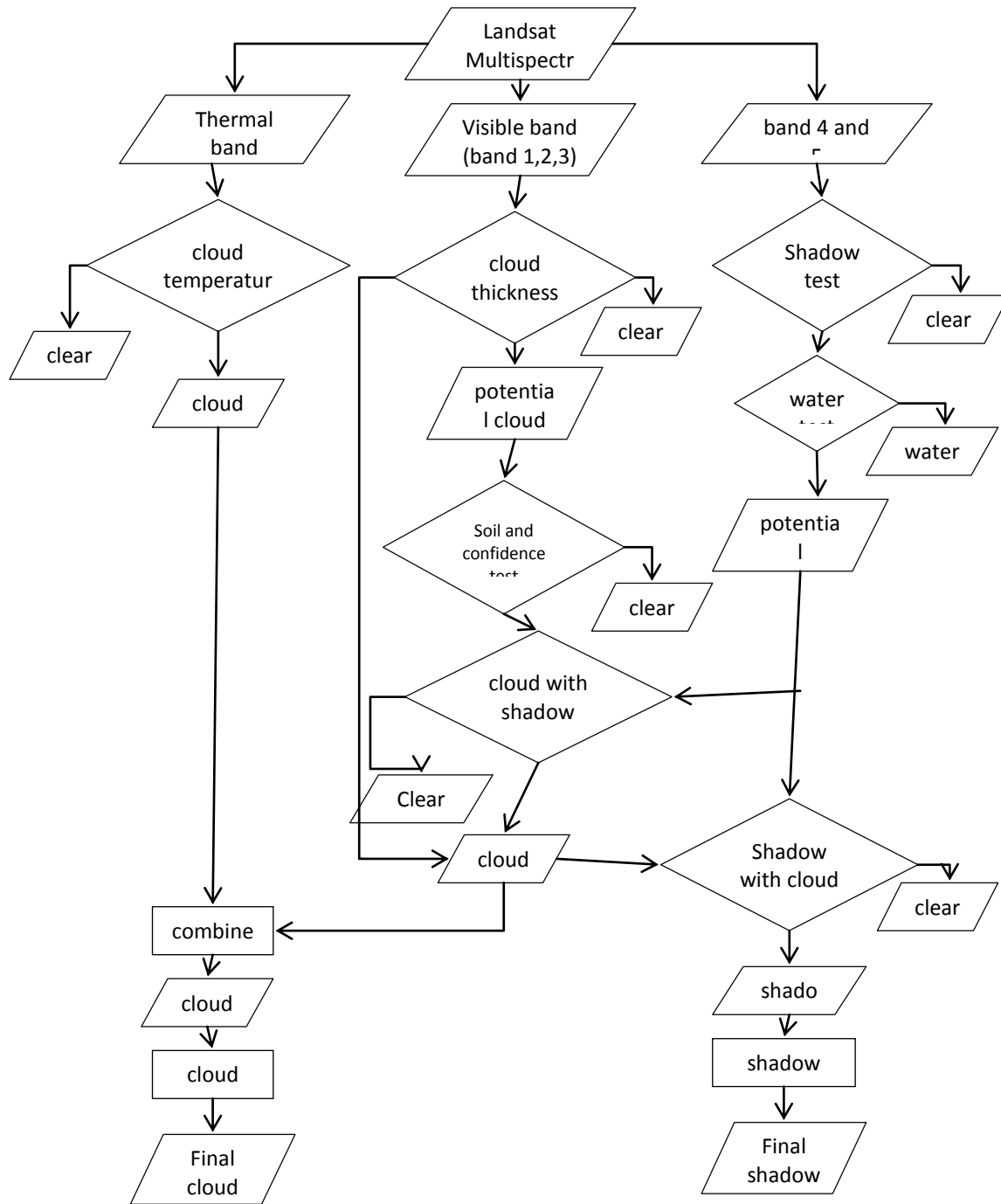


Figure 1. Flowchart of cloud and cloud shadow masking

distinguish bare soil from cloud pixels. The condition and equation were as follows:

if $f(X)_{soil} > X_{soil-thres}$, then $P = \text{cloud}$ pixels, otherwise was classified as soil.

Where:

soil test function:

$$f(X)_{soil} = 2 * X_1 - X_2 - X_3 + 2 * X_4 - 2 * X_5;$$

$X_i = \text{digital number for Pixel band -i of Landsat data}$

$X_{soil-thres} = \text{soil and cloud threshold value}$

$P = \text{pixel}$

Confidence Test was a test to measure the distance of closeness to cloud. If the distance of the probably cloud to the absolutely cloud pixels less then five pixels, the probably cloud were classified to absolutely cloud pixels, otherwise were classified to probably cloud pixels. Finally,

this algorithm will spatially improve the cloud mask by using the rule that sets a pixel to cloud if five or more pixels in its 3-by-3 neighborhood are cloud pixels; otherwise, the pixel stays clear.

2.2.2 Potential cloud shadow layer

Since the beam of solar radiation was blocked by the clouds, the cloud shadows were mainly illuminated by scattered light. As the atmospheric scattering was stronger at shorter wavelengths (for example visible bands), the diffusive radiation in the shadows would be relatively smaller at longer wavelengths (for example NIR and SWIR bands), making the shadowed pixels darker than their surroundings (Luo *et al.*, 2008). Moreover, as NIR reflectance was usually high (including vegetation and rock), the darkening effect of cloud shadows was most obvious in this band.

The test for cloud shadow detection was as follows:

if $f(X)_{cloud-shadow} \leq X_{shadow-thres}$, then P was classified as probably shadow pixels; otherwise was classified absolutely non shadow pixels;

where:

$$f(X)_{cloud-shadow} = X_4 + X_5;$$

X_i : digital number for fixel band -i of Landsat data

$X_{shadow-thres}$ = shadow threshold value

P = pixel

If the result was probably shadow pixel, the water test was then applied. The water test was used to separate water and probable shadow pixels, as follows:

If $f(X)_{shadow-water} < X_{water-thres}$, then P was classified as water, otherwise was classified as shadow.

Where:

Shadow function:

$$f(X)_{shadow-water} = (X_2 + X_3 - X_5);$$

X_i : digital number for fixel band -i of Landsat data

$X_{water-thres}$ = shadow and water threshold value

P = pixel

2.2.3 Geometric relationship between cloud and cloud shadow match

The basic idea of cloud and cloud shadow matching approach was that by knowing the view angle of the satellite sensor, the solar zenith angle, the solar azimuth angle, and the relative height of the cloud, we can predict the cloud shadow location based on the geometric relationship between cloud pixels and respective shadow pixels. Once the first three factors were known, we could use them to calculate the projected direction of the cloud shadow. Along this direction, the algorithm matched the cloud object with the potential shadow layer since a cloud and its shadow must be in the projected direction (Figure 2).

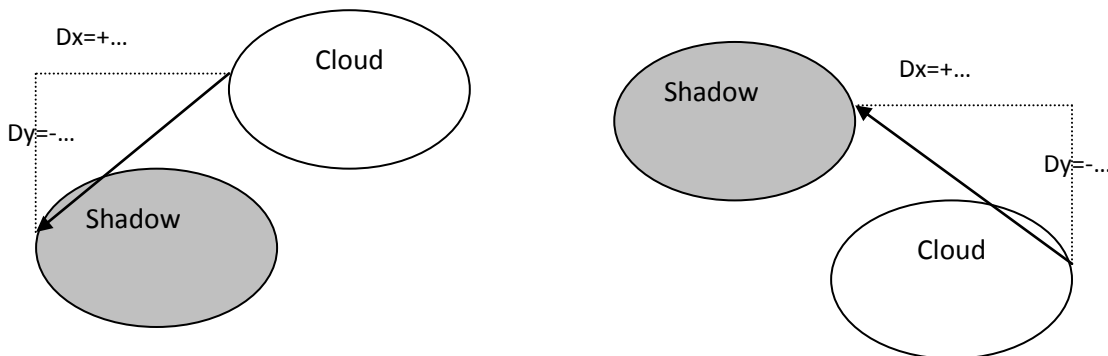


Figure 2. Schematic of spatial relationship between the potential cloud and shadow. Dx= easting distance between position of cloud and shadow pixel; Dy= northing distance between position of cloud and shadow pixel.

The cloud height was estimated by cloud size. The cloud size were categorized to three categories i.e., 1-30 pixels, 31-50 pixels, and >50 pixels. If cloud size were 1-30 pixels, the shadow distance from cloud was 0-20 pixels, if cloud size were 31-50 pixels, the shadow distance from cloud was 0-30 pixels, and if cloud size more than 50 pixel, the searching distance of shadow was 0-200 pixels.

As cloud base height could be any value from approximately 200 m to 12,000 m, it would be time consuming and may cause false matches if we iterated cloud height across the entire range for every single cloud object to find its shadow. Therefore, it was very essential to develop a method, which could be more efficiently encountered a huge number of pixels as well as a big volume of satellite data.

3 RESULT AND DISCUSSION

3.1 Cloud and cloud shadow mask

The results of cloud and cloud shadow detection of Landsat imagery of 10 May 2001 scene 124-062 in false color composites background are presented in Figure 3, 4, and 5. The cloud could be identified clearly as appeared in red from

albedo (Figure 3) and yellow from thermal band (Figure 4), while the cloud shadow appeared in magenta (Figure 5). Albedo was used to identify the cloud thickness, while thermal band was used to identify the cloud height. The higher the cloud the lower the temperature of cloud. Thin cloud usually had the lower temperature, so the thin cloud was detected easily by thermal band.

In this subset image, there were two types of clouds, thin cloud and thick cloud. White clouds (thick cloud) could be detected by albedo and thin clouds could be detected by thermal band. Combining these two kinds of cloud, thick and thin cloud, into cloud can be shown in Figure 6 and 7 in white color.

Cloud shadow as shown in Figure 5 showed many errors, the red circles were not real cloud shadow but detected as cloud shadow. By combining the cloud and cloud shadow, we could obtain a better result as seen in Figure 6. After applying geometric relationship method on cloud and cloud shadow, it showed that shadows without cloud could be eliminated as seen in Figure 7. Small thick cloud in Figure 7 with the red circle was also detected using this method where every small thick clouds always have a shadow of their association.

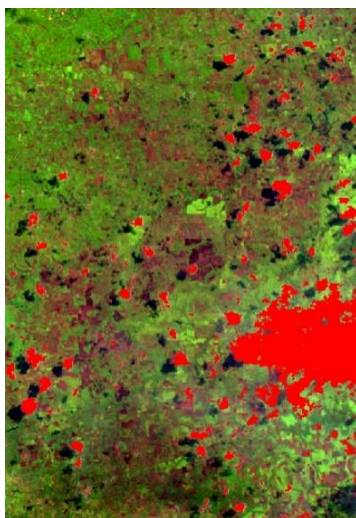


Figure 3. Cloud detection from albedo test.



Figure 4. Cloud detection from thermal test.

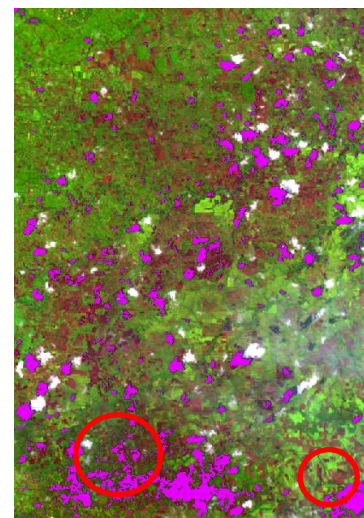


Figure 5. Shadow detection

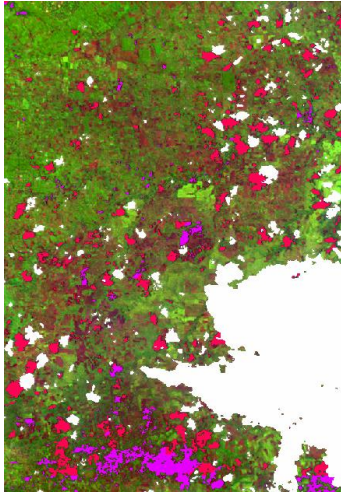


Figure 6. Cloud and shadow detection before geometric relationship processing.



Figure 7. Cloud and shadow detection after geometric relationship processing.

White : Cloud
 Red : Shadow
 Magenta : shadow without cloud

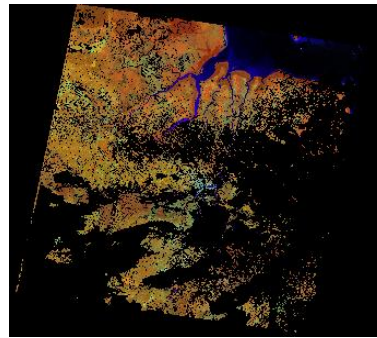
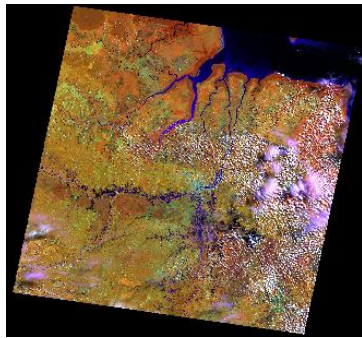


Figure 8. Landsat 7 imagery scene 124062, date 100501 (left), cloud masking result (right).

Table 2. Accuracy assessment result from Landsat 7 imagery scene 124062, date 100501.

Classes	Cloud	Non Cloud	Total
Cloud	36256869 pixels (62.94 %)	16030 pixels (0.03 %)	36272899 pixels (62.97%)
Non Cloud	705151 pixels (1.22%)	20627150 pixels (35.81%)	21332301 pixels (37.03%)
Total	36962020 pixels (64.16%)	20643180 pixels (35.84%)	57605200 pixels (100.00%)

The accuracy assessment of the cloud and cloud shadow result was investigated by applying the method for whole scenes of Landsat imagery that cloud be seen in Figure 8. The accuracy result in Table 2 showed that 36256869 pixels (62.94 %) of cloud remained cloud, and 20627150 pixels (35.81 %) of non cloud remained non cloud, so the 98.75 % of pixel well detected. The error result was 1.25 %, if this error was separated

into commission and omission errors, the commission error was 1.22 %, and the omission error was 0.03 %. The omission error more important compared with commission error. If commission error was detected, the missing area could be change with the same data in difference date of acquisition, but if omission error was detected, the error could not be removed.

3.2 Comparison with other method

We also compared the result of cloud and cloud shadow using this method with the cloud and cloud shadow using tree base algorithm from Maryland University. Figure 9a showed the result from of this method, Figure 9b was the original Landsat imagery in RGB 321 composite, and Figure 9c was the result from tree base algorithm. Another comparison in difference area are also shown in Figure 10. Figure 10a showed the result from of this method, Figure 10b was the original Landsat imagery in RGB 321 composite, and Figure 10c was the result from tree base algorithm.

The area inside red circle in Figure 9c and 10c showed that there were some

misleading results of the tree base method, in which the river flow was identified as shadow. As an example, the water surface on the right below side of the subset in Figure 9b, could be distinguished from cloud shadow using this method (Figure 9a), but identified as cloud or cloud shadow using the tree base method (Figure 9c). From the above figures it was also revealed that this method could effectively detect clouds and cloud shadows, which enabled to perform an automated data processing. Therefore the method proposed by this study could be used to undertake cloud masking or screening of satellite data more easily.

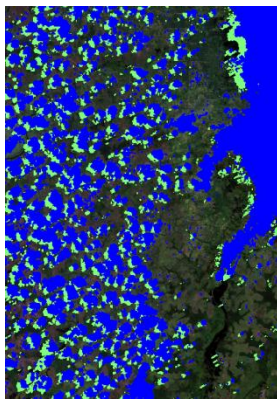


Figure 9a. Cloud and shadow mask from this method.



Figure 9b. Composite 321 Landsat.

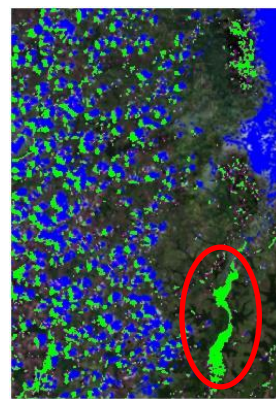


Figure 9c. Cloud and shadow mask from tree base method.

Legend:
Blue/white :
Clouds
Green : Shadows

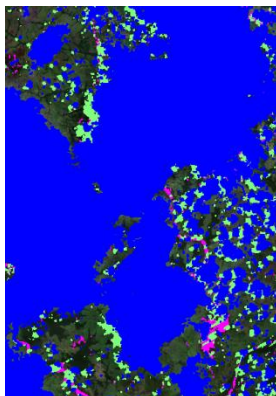


Figure 10a. Cloud and shadow mask from this method.



Figure 10b. Composite 321 Landsat.



Figure 10c. Cloud and shadow mask from tree base method.

Legend:
Blue/white :
Clouds
Green : Shadows

4 CONCLUSION

The estimates of cloud cover derived from this algorithm provided improvement results compared with using tree base algorithm estimation. There are two types of clouds which could potentially result misleading identification i.e., thin clouds and small thick clouds which were usually difficult to be detected by many methods. However they could be identified very well by this method. Water surface was among of the object which could have similarities with cloud shadow features, but they could be distinguished quite well using this proposed method. Meanwhile that object with similar features could not be distinguished by the tree base algorithm method accurately. The accuracy result of this method was 98.75%.

REFERENCES

- Ackerman, S.A., K.I. Strabala, W.P. Menzel, R.A. Frey, C.C. Moeller, and L.E. Gumley, 1998, Discriminating clear sky from clouds with MODIS, *Journal of Geophysical Research*, 103(24): 32141–32157.
- Arvidson, T., J. Gasch, and S.N. Goward, 2001, Landsat-7's long-term acquisition plan An innovative approach to building a global imagery archive, *Remote Sensing of Environment*, 78(1–2):13–26.
- Asner, G.P., 2001, Cloud cover in Landsat observation of the Brazilian Amazon. *International Journal of Remote Sensing*, 22(18):3855–3862.
- Berendes, T., S.K. Sengupta, R.M. Welch, G.A. Wielicki, and M. Navar, 1992, Cumulus cloud base height estimation from high spatial resolution Landsat data: A Houghtransform approach, *IEEE Transactions on Geoscience and Remote Sensing*, 30:430–443.
- Derrien, M., B. Farki, L. Harang, H. LeGleau, A. Noyalet, D. Pochic, and A. Sairouni, 1993, Automatic cloud detection applied to NOAA-11/ AVHRR imagery, *Remote Sensing of Environment*, 46(3):246–267.
- Gao, B.C., and Y.J. Kaufman, 1995, Selection of the 1.375- μm MODIS channel for remotesensing of cirrus clouds and stratospheric aerosols from space, *American Meteorological Society*, 52:4231–4237.
- Gao, B.C., Y.J. Kaufman, W. Han, and W.J. Wiscombe, 1998, Correction of thin cirrus path radiance in the 0.4–1.0 μm spectral region using the sensitive 1.375 μm cirrus detecting channel, *Journal of Geophysical Research*, 103(24):32169–32176.
- Gao, B.C., P. Yang, W. Han, R.R. Li and W.J. Wiscombe, 2002, An algorithm using visible and 1.38- μm channels to retrieve cirrus cloud reflectances from aircraft and satellite data, *IEEE Transactions on Geoscience and Remote Sensing*, 40(8):1659–1668.
- Hégarat-Masclé, S.L., and C. André, 2009, Use of markov random fields for automatic cloud/shadow detection on high resolution optical images, *ISPRS Journal of Photogrammetry and Remote Sensing*, 64:351–366.
- Hutchison, K.D., R.L. Mahoney, E.F. Vermote, T.J. Kopp, J.M. Jackson, A. Sei, and B.D. Iisager, 2009, A geometry-based approach to identifying cloud shadows in the VIIRS cloud mask algorithm for NPOESS, *Journal of Atmospheric and Oceanic Technology*, 26(7):1388–1397.
- Irish, R., 2000, Landsat-7 automatic cloud cover assessment algorithms for multispectral, hyperspectral, and ultraspectral imagery. *The International Society for Optical Engineering*, 4049:348–355.
- Irish, R., J.L. Barker, S.N. Goward and T. Arvidson, 2006, Characterization of the Landsat-7 ETM+ Automated Cloud-Cover Assessment (ACCA) algorithm, *Photogrammetric Engineering and Remote Sensing*, 72(10):1179–1188.
- Luo, Y., A.P. Trishchenko, and K.V. Khlopenkov, 2008, Developing clear-sky, cloud and cloud shadow mask for

- producing clear-sky composites at 250-meter spatial resolution for the seven MODIS land bands over Canada and North America, *Remote Sensing of Environment*, 112(12):4167-4185.
- Oreopoulos, L., M. Wilson, and T. Várnai, 2011, Implementation on Landsat data of a simple cloud mask algorithm developed for MODIS land bands, *IEEE Transactions on Geoscience and Remote Sensing*, 8(4):597–601.
- Saunders, R.W., and K.T. Kriebel, 1998, An improved method for detecting clear sky and cloudy radiances from AVHRR data, *International Journal of Remote Sensing*, 9(1):123–150.
- Simpson, J.J. and J.R. Stitt, 1998, A procedure for the detection and removal of cloud shadow from AVHRR data over land, *Geoscience and Remote Sensing*, 36(3):880–890.
- Simpson, J.J., J.R. Stitt and Z. Jin, 2000, Cloud shadow detection under arbitrary viewing and illumination conditions, *IEEE Transactions on Geoscience and Remote Sensing*, 36:880–897.
- Vermote, E., 2010, Landsat Science Team Meeting Mountain View, California, USA.
- Vermote, E., and N. Saleous, 2007, LEDAPS surface reflectance product description, Version 2.0.
- Wang, B., A. Ono, K. Muramatsu, and N. Fujiwara, 1999, Automated detection and removal of clouds and their shadows from Landsat TM images. *IEICE Transactions on Information and Systems*, 82(2):453-460.
- Zhang, Y., B. Guindon, and J. Cihlar, 2002, An image transform to change characterize and compensate for spatial variability in thin cloud contamination of Landsat images, *Remote Sensing of Environment*, 82(2–3):173–187.

